POLITECNICO
MILANO 1863

SCUOLA DI INGEGNERIA INDUSTRIALE
E DELL'INFORMAZIONE

EXECUTIVE SUMMARY OF THE THESIS

Design and validation of new Accelerated Stress Tests for the experimental analysis of hydrogen PEM fuel cell degradation under real world automotive operation

TESI MAGISTRALE IN ENERGY ENGINEERING – INGEGNERIA ENERGETICA

AUTHOR: DANIELE MORA

ADVISOR: ANDREA CASALEGNO

ACADEMIC YEAR: 2020-2021

1. Introduction

Durability is one of the main issues that limits the diffusion of polymer electrolyte membrane (PEM) fuel cells in automotive applications. The degradation can affect several components of the PEM fuel cell, such as the membrane, the Pt catalyst or the carbon support of the electrode. In real-world automotive applications, PEMFCs usually face very heterogeneous operating conditions, that lead to heterogeneous degradation. In automotive applications, it is possible to distinguish between two main operative conditions: Low Power operation, typical of urban load cycles, and High Power operation, where maximum power output is requested to the fuel cell system. Inside the Horizon 2020 European project ID-FAST, in the frame of which this thesis is developed, a reference driving cycle was designed according to real data available at project's partners. The aim of this European project it to support and promote PEMFCs for vehicles, through the development of Accelerated Stress Tests (AST) that are able to predict the ageing in real world functioning and accelerating the introduction of innovative materials in next generation designs.

ASTs are a very important tool to reduce the operative time required to evaluate the durability of materials: the current state of art AST, however, are usually related on single degradation mechanisms [1]. The current state of art ASTs are focused on catalyst degradation, carbon support corrosion and membrane's mechanical and chemical degradation. The first two are performed in H_2/N_2 atmosphere, while membrane AST keeps steady state OCV conditions for chemical degradation and adds relative humidity cycles to induce mechanical degradation. Some recent studies consider operative conditions more representative of automotive application: Zihrul et al. [2] and Kneer et al. [3–5] investigated the catalyst degradation under H_2/air feed, focusing on the separate effects caused by few stressors, such as UPL (Upper Potential Limit), dwell time at UPL, scan rate, temperature and relative humidity.

The aim of this work is to study the single MEA degradation under controlled operative conditions representative of real automotive operation, and to develop ASTs that are representative of real degradation for specific operational modes. The

control of the operative conditions allows to reproduce local degradation of real hardware.
To do so, specific AST for Low Power and High Power operations are designed and analyzed. Then, a Combined AST is developed with the aim of evaluating the impact on degradation caused by the combination of the two different operations. The results are then validated on complete ID-FAST driving cycle of 1000 operating hours, realized in previous work at *MRT Fuel Cell & Battery Lab* [6]. Furthermore, the degradation originated by the realistic operations is investigated. The work relies on the zero-gradient cell hardware, which was developed at Politecnico di Milano, to operate the Membrane Electrode Assemblies (MEA) in homogeneous conditions over the cell area [7]. It was adopted a particular configuration of the zero-gradient cell that allowed to simultaneously test four different MEA's. The description of the hardware configuration and its validation are presented in Chapter 2 of the thesis. A modeling activity is performed on the data obtained from the experimental analysis, to better evaluate the impact of catalyst active area reduction on the performance loss measured during the newly developed ASTs.

2. Catalyst durability under D.o.E. Electrocatalyst AST

One of the main source of performance loss in a PEMFC during operation is related to the reduction of electrochemically active surface area (ECSA) of the Pt catalyst. The US Department of Energy (D.o.E.) Electrocatalyst AST is designed to assess cathode electrocatalyst durability through the use of a voltage square wave, maximizing catalyst degradation while minimizing support corrosion [1]. Therefore it was applied on four different MEA's to have a comparison reference for the automotive ASTs that will be designed. Despite some differences in materials characteristics (refer to section 2.1.1), the ECSA loss measured during this test was comparable for the MEA's. The minimum ECSA reached after 75,000 AST cycles was between 34%, for MEA A, and 45%, for MEA D, of Beginning of Test (BoT) values. It seems that a stable condition is not reach at the End of Test (EoT). The Mass Transport Resistance (RMT) was evaluated from limiting current measurements [8]. Only the pressure independent component of the resistance increased after the ageing protocol (refer to section 3.2.3 for a deeper analysis).

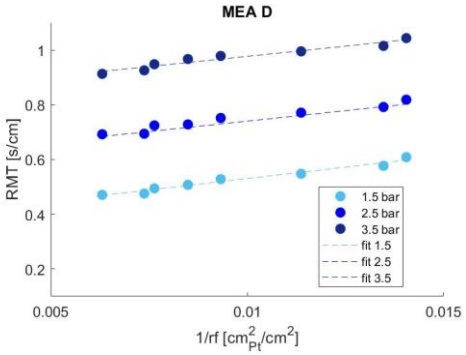

Figure 1: RMT as function of the roughness factor for MEA D during Electrocatalyst AST degradation; only MEA D was reported for sake of simplicity

As reported in Figure 1, a linear relation was also found between the RMT and the inverse of the roughness factor, which is a parameter proportional to the ECSA. The measured values of the chart slope, reported in Table 1, are in good agreement with the literature [9]. The linear relation allows to identify in the chart slope the local transport resistance at the Pt surface, originated from the interfacial transport through the ionomer film, while excluding structural alterations as due to support corrosion [7].

Test	**MEA A**	**MEA B**	**MEA C**	**MEA D**
Pt AST	13.74	13.26	9.35	15.61
LP	19.69	14.17	7.89	13.65
HP	17.49	15.89	8.20	13.18
Comb	18.56	15.58	12.89	16.21

Table 1: Values of calculated local oxygen resistance for each MEA during the performed ASTs expressed in [s/cm]

3. Design of Low Power and High Power AST and degradation analysis

The Low Power AST and High Power AST were designed considering the ID-FAST driving cycle operating conditions as a starting reference. Both ASTs were performed in H_2/air atmosphere: this allowed to include in the test the effects of proton and electron conduction and heat generated by electrochemical reactions, with respect to protocols

performed in inert atmosphere. For the protocol definition of Low Power and High Power AST, it was decided to reproduce as closely as possible the main stressors that characterized the two operative conditions: voltage profile, relative humidity (RH), temperature and pressure (Figure 2). The chosen operative conditions are representative of average operation of real fuel cell stacks.

For Low Power (LP) AST, pressure and temperature were kept constant and the gas feed had a RH of 70% and 60% for anode and cathode respectively. Cell temperature was set equal to 71 °C. Since closer to real functioning, AST were designed as galvanostatic operations, meaning that the current is imposed and the resulting voltage recorded. Current setpoints are specific for each material and selected to ensure typical constraints in voltage profile at BoT: an asymmetrical square wave between and Upper Potential Limit (UPL) of 0.85 V and a Lower Potential Limit (LPL) of 0.7 V, repeated 6 times. Dwell time was 30 s at UPL and 12 s at LPL. The galvanostatic load profile is reported in Figure 2 (dotted grey lines), as well as the potential profile resulting at BoT (green lines). At the end, a short stop procedure was introduced: cathode gas feed is closed and potential drops below 0.1 V.

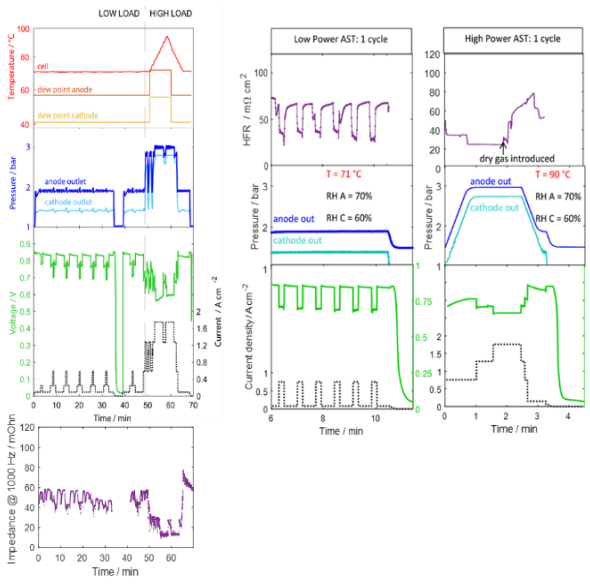

Figure 2: ID-FAST driving cycle operating conditions (left); Low Power AST (middle) and High Power AST (right) conditions

For the High Power (HP) AST, temperature was set constant to 90 °C, reproducing the realistic, most stressful condition. Gas feed RH was the same as Low Power AST, but in this case to reproduce the large humidity cycling stressor recorded during the driving cycle, a switch to dry cathode feed was realized towards the end of each cycle. The impedance profile of the driving cycle in Figure 2 (purple line) was reproduced during the HP AST (right side of Figure 2), considering how the high frequency impedance provides information regarding the hydration state of the MEA. Also, high power operation was characterized by a variable pressure, therefore a wide pressure cycling was introduced. Again, the galvanostatic profile was specifically set to obtain a voltage profile which resumes the realistic operation, in the range 0.65 V - 0.85 V at BoT. Similarly to the Low Power AST, a short stop is performed at the end of each High Power cycle.

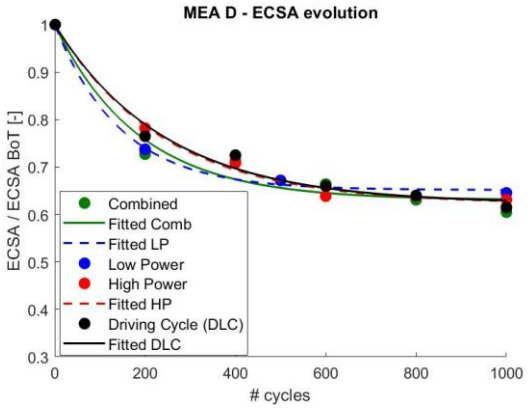

Figure 3: ECSA ageing during Low Power, High Power, Combined AST and ID-FAST Driving Cycle for MEA D

1,000 cycles of both LP and HP AST were tested on the same four MEA's. The loss of catalyst active area was comparable between the two tests: the ECSA recorded at EoT was between 57% and 71% of the BoT in dependence of the material type. Furthermore, as also shown in Figure 3, the ECSA is approaching a stable conditions, differently than what observed during D.o.E Electrocatalyst AST. Overall, the ECSA loss was lower compared to the Electrocatalyst AST, probably due to the different UPL, which is a stressor that plays a major role in catalyst degradation [2][4] and due to the different holding times.

Performance characterization was performed with polarization curves: these are procedures where the current is imposed and the resulting voltage is measured. Therefore, the performance loss was evaluated as the voltage difference, at each current value, between BoT and EoT recorded curves (at 80

°C in H_2/air atmosphere). Performance characterization is performed after a cathode cleaning procedure, described in section 2.3.2 of the thesis, that involves a Cyclic Voltammetry with 1.2 V as UPL: in this way it is possible to remove contaminants from cathode and recover reversible losses. Voltage losses are summarized in Figure 4. Voltage losses at the end of Low Power AST were almost constant with the current density, suggesting that the loss of ECSA was the main degradation mechanism affecting the MEA's. For MEA D the losses reduced in the medium currents region: this could be attributed to a reorganization of the ionomer in the catalyst layer or some heterogeneities effects caused by degradation. High Power caused a higher degradation compared to the previous test. The main difference with LP AST was observed in the medium/high currents region: for MEA A, B and C it seemed that the additional losses were linearly proportional to the current density (ohmic behavior), while for MEA D losses had a more exponential trend, suggesting that they were related to mass transport effects. The mass transport resistance kept a linear trend with respect to the roughness factor (Table 1), so it can be concluded that no support decay occurred during these ASTs [10].

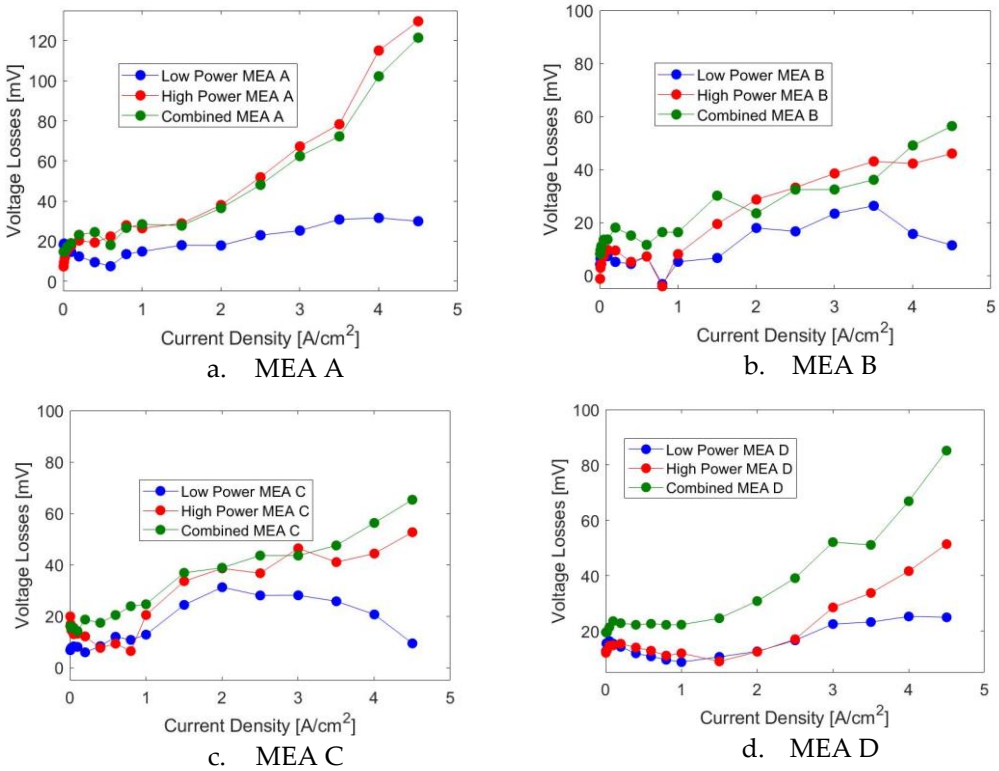

Figure 4: Voltage losses recorded at the end of each AST on reference polarization curve (80°C and hydrogen air atmosphere) for tested MEA's

The Electrochemical Impedance Spectroscopy (EIS), performed in the same conditions as the polarization curve, confirmed the higher impact of High Power on mass transport, with the Low Frequency Resistance being higher than the Low Power AST (Figure 5). The High Frequency Resistance, instead, showed no significant changes at EoT, therefore the cause for the ohmic losses of MEA A, B and C was not related to a membrane degradation. To evaluate the impact of degradation on catalyst layer ionic resistance, EIS were performed at ambient temperature and inert atmosphere. With this procedure it is possible to highlight the linear behavior at high frequencies that provides an indication on the ionic resistance of catalyst layer [11].

A higher projection of the linear branch onto the real axis denotes a higher ionic resistance. However, the high frequency response was not linear, but it appeared that an additional arc arose at the end of the test, as clearly shown in Figure 6. This suggested that for these MEA's, the losses were related to an increase in the anode

overpotential. An anode cleaning procedure was designed to verify the anode contribution.

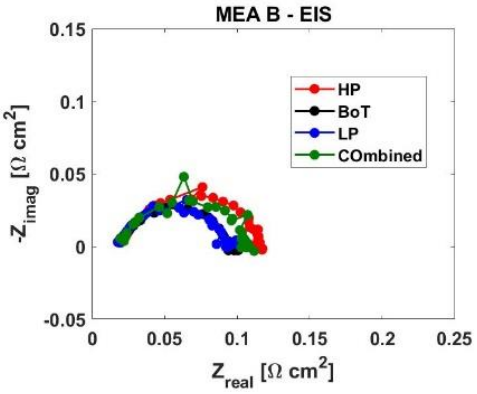

Figure 5: EIS at 3 A/cm^2 on reference polarization curve condition at the end of each AST. Only MEA B is here reported for the sake of simplicity. Applied frequencies follow a logarithmic distribution between a maximum of 20 kHz and a minimum of 1 Hz.

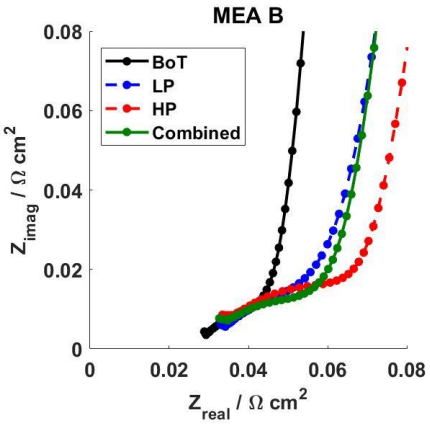

Figure 6: EIS performed at ambient temperature and inert atmosphere. It is possible to observe the high frequency arc at the end of HP AST and Combined AST. Only MEA B is here reported for the sake of simplicity. The range of considered frequencies is again from 20 kHz to 1 Hz

3.1. Cleaning of anode catalyst layer

The complete anode refresh procedure is describe in section 4.4.1 of the thesis and it is similar to cathode cleaning procedure. The gas feeds were switched: N_2 was fed to the anode and H_2 to the cathode. The core of the procedure was a cleaning CV (section 2.2.1) characterized by an UPL equal to 1.2 V, with the aim to remove possible contaminants that could inhibit anode catalyst activity. An example of cleaning CV is reported in Figure 7. The procedure seemed to activate the Pt active surface of anode catalyst layer. Furthermore, at high voltage the behavior of consecutive scans suggested a possible contaminants desorption. CO poisoning was not excluded as possible degradation due to the current limits of the refresh procedure: air leakages at the anode side can oxidate the CO before the application of the cleaning CV.

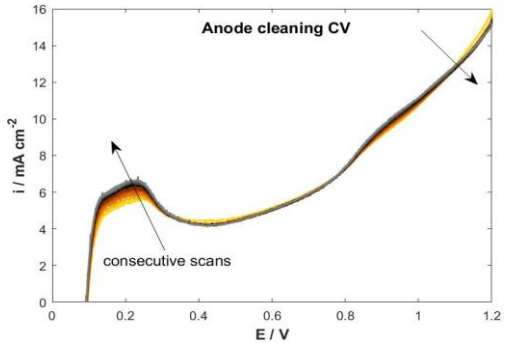

Figure 7: Example of anode cleaning CV. The arrows indicates the ten consecutive scans, from the first one to the last one

The anode refresh procedure was applied to both LP and HP samples. The EIS in inert atmosphere did not shown anymore the high frequency arc after the refresh procedure. Therefore it was possible to conclude that the observed anode degradation was reversible. MEA A, B and C showed only small performance recovery for the Low Power AST, while on High Power AST the recovery was more significant, especially on MEA A. MEA D, instead, seemed not to be affected by the procedure.

After the anode cleaning, it appeared that for both LP AST and HP AST the main cause of degradation was the loss of catalyst active area, with also some additional minor losses in the medium/high currents region for the High Power AST that could be attributed to a different degradation induced in the cathode catalyst layer by the different stressing operative conditions.

4. Combined AST

A Combined AST was developed in order to take into account the effects given by the coupling of Low Power and High Power operation as in real driving and shown in the reference driving cycle of Figure 2. 1 Combined AST cycle is given by 1 LP AST cycle and 1 HP AST cycle. The Combined AST protocol consists in the alternation of 200 Low

Power cycles with 200 High Power cycles: alternating 1 single LP cycle with 1 single HP cycle was not feasible due to the time required to regulate the operating temperatures.
A first sample was tested up to 1,000 Combined AST cycles, in order to have a direct comparison with the previous single-mode ASTs. Figure 3 shows that the trend of ECSA loss was comparable with the two previous tests. The voltage losses measured before the anode refresh were already reported in Figure 4 . For MEA A, B and C the losses observed during the Combined AST were very close to the ones of the High Power AST. Considering MEA D, instead, the profile was again closer to High Power AST, but the losses were more important for the Combined AST. Despite the similar losses, from the EIS of Figure 6. it seemed that the combination of Low Power cycles and High Power cycles mitigated the anode degradation.
MEA A, B and C confirmed a degradation similar to High Power AST even after the anode refresh procedure: the major contribution to the performance decay can again be attributed to the loss of ECSA with some minor additional losses in the medium/high current densities region.
A second sample was tested under Combined AST protocol. MEA A, B and D showed very comparable ECSA decay and voltage losses, proving the great repeatability of the Combined AST protocol.
As previously described, results were compared to the whole 1000 hours of ID-FAST driving cycle. The loss of catalyst active are is reported in Figure 3 for MEA D, and its evolution over time was very well represented by the newly developed Combined AST. Similar results were obtained also for MEA A and MEA B, not here reported but presented in section 5.4 of the thesis.

Condition	MEA A	MEA B	MEA D
DLC 0.78V	22.7	8.0	38.5
DLC 0.65V	63.2	28.8	72.5
Comb 0.78V	22.1	10.8	21.6
Comb 0.65V	63.6	30.5	48.9
Comb_v2 0.78V	21.2	13.2	21.3
Comb_v2 0.65V	60.8	29.5	46.3

Table 2: Voltage loss comparison between ID-FAST driving cycle (DLC) and the Combined AST performed on two samples. Results are expressed in mV

Table 2 summarizes the voltage loss on reference polarization curve for the ID-FAST driving cycle (DLC) and both Combined ASTs. Since the flowfield design and the stoichiometries adopted were different among the adopted hardware, it was decided to choose two reference currents on which evaluate the voltage losses, one representative of low currents region of polarization curve and the other for the high currents region. It was decided to select two points that satisfied the criterion of the same BoT voltage: 0.78 V and 0.65 V. The results showed that the Combined AST was representative of real degradation.

5. Modeling of performance ageing

A 1D model was used in this work to further study the degradation measured during the experimental tests. The model was previously developed and tested during other activities. Only MEA D was considered due to the fact that it was extensively tested and studied within the laboratory, and the model was calibrated on its characteristics. The first part of the modeling activity was to reproduce the performance loss caused by the reduction of ECSA during the Electrocatalyst AST. In Figure 8 both experimental and simulated polarization curves at BoT and EoT are presented. It is possible to observe how the model shows a very good capability of reproducing ECSA loss effects.

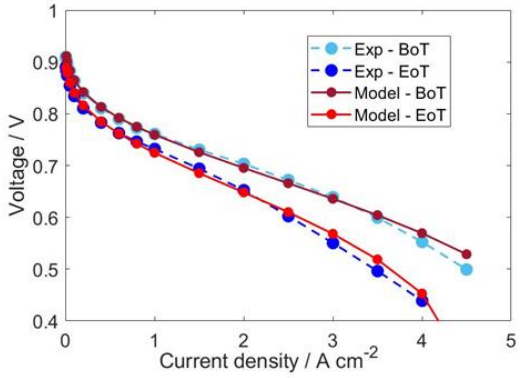

Figure 8: Comparison between experimental (blue curves) and simulated (red curves) reference polarization curves at BoT and EoT of Electrocatalyst AST for MEA D

The model was then applied to LP AST, HP AST and Combined AST. The voltage losses are

reported in Figure 9. The simulated profile was very similar to the one of the experimental measurements for both Combined AST and High Power AST, confirming how the ECSA loss was the major cause for performance decay. However, it seems that the model slightly underestimates the losses at medium/high current densities, suggesting the presence of additional losses in this region. For the Low Power AST instead, the losses in the mass transport region are overestimated by the model. A possible explanation for the minor differences observed could be attributed to the evolution of Pt nanoparticles during ageing caused by the different operating conditions that characterize ASTs operations or a different stressing of catalyst layer structure that changes mass transport properties at high current densities (i.e. related to ionomer configuration).

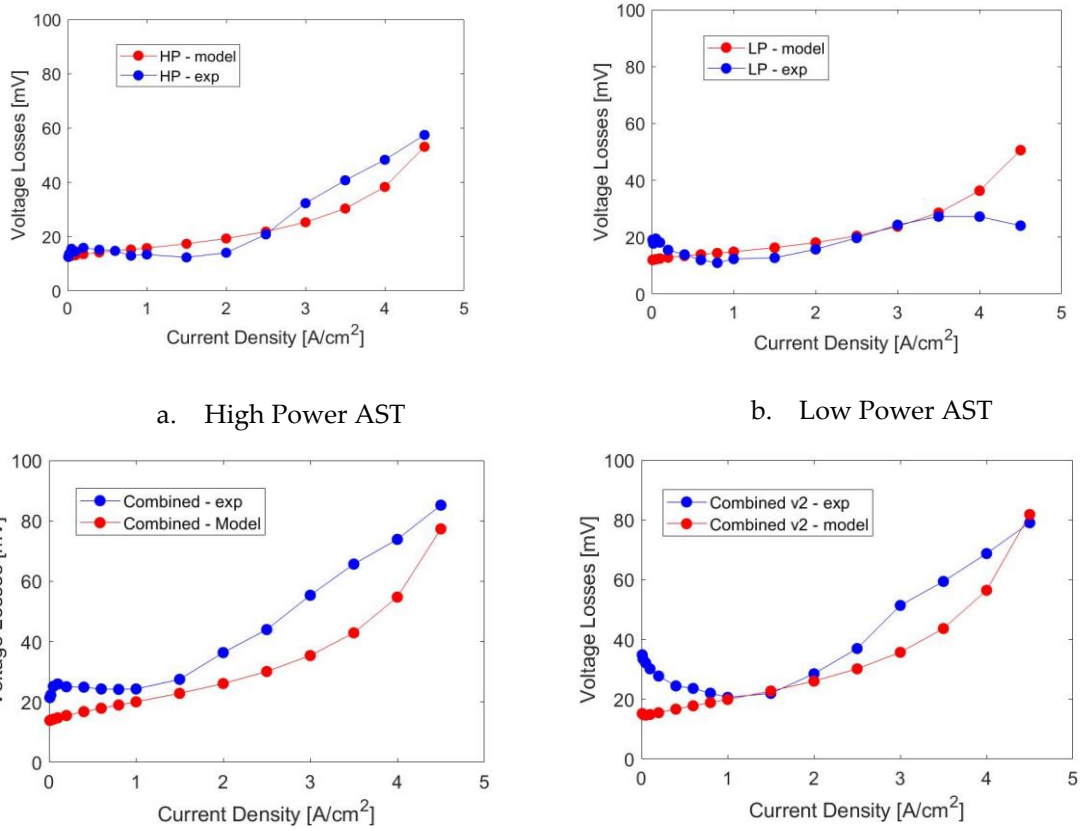

a. High Power AST

b. Low Power AST

c. Combined AST

d. Combined AST v2

Figure 9: comparison between experimental (blue lines) and simulated (red lines) voltage losses at the end of the newly developed ASTs

6. Conclusions

This work aimed to analyze the effect on PEMFC degradation under typical automotive operating conditions. To do so, two specific Accelerated Stress Tests were developed, one for Low Power and one for High Power operation. They were performed over various MEA's and different performance losses were recorded, with the High Power operation being the most stressful. One degradation mechanism observed during High Power AST was attributed to the anode and a specific procedure was design to recover the reversible losses. The High Power AST, characterized by higher temperatures, pressures and changes between humidified/dry gas feeding, was proven to be the most stressful even after the recovery procedure.

A Combined AST was then designed to study the effects of coupling the two operating conditions and to reproduce the degradation observed in previous work after the application of a long-term testing driving cycle.

Combined AST showed a very good repeatability when performed on a second sample, and a comparison with the ID-FAST driving cycle showed also a very good capability of reproducing real degradation. The calculated acceleration factor, in terms of total testing time, was equivalent

to x9.5. Validation was carried out both in terms of ECSA loss and irreversible voltage decay.
A 1D model was used to further study the degradation. After a comparison and calibration with the results obtained from simulation of D.o.E. Electrocatalyst AST it was possible to conclude that the major contribute to the degradation was related to loss of catalyst active area, with minor additional losses affecting the performance in High Power AST and Combined AST, in the operational region where mass transport phenomena have an impact.

References

[1] U.D. of Energy (DOE), Fuel Cells 2016 - Multiyear research, development, and demonstration plan, (2016). http://energy.gov/sites/prod/files/2015/10/f27/fcto_2014_market_report.pdf.,https://www.daimler.com/documents/company/other/daimler-corporateprofile-en-2015.pdf.

[2] P. Zihrul, I. Hartung, S. Kirsch, G. Huebner, F. Hasché, H.A. Gasteiger, Voltage Cycling Induced Losses in Electrochemically Active Surface Area and in H 2 /Air-Performance of PEM Fuel Cells , J. Electrochem. Soc. 163 (2016) F492–F498. https://doi.org/10.1149/2.0561606jes.

[3] A. Kneer, N. Wagner, C. Sadeler, A.-C. Scherzer, D. Gerteisen, Effect of Dwell Time and Scan Rate during Voltage Cycling on Catalyst Degradation in PEM Fuel Cells, J. Electrochem. Soc. 165 (2018) F805–F812. https://doi.org/10.1149/2.0651810jes.

[4] A. Kneer, N. Wagner, A Semi-Empirical Catalyst Degradation Model Based on Voltage Cycling under Automotive Operating Conditions in PEM Fuel Cells, J. Electrochem. Soc. 166 (2019) F120–F127. https://doi.org/10.1149/2.0641902jes.

[5] A. Kneer, J. Jankovic, D. Susac, A. Putz, N. Wagner, M. Sabharwal, M. Secanell, Correlation of Changes in Electrochemical and Structural Parameters due to Voltage Cycling Induced Degradation in PEM Fuel Cells, J. Electrochem. Soc. 165 (2018) F3241–F3250. https://doi.org/10.1149/2.0271806jes.

[6] E. Astori, D. Cecile, Automotive PEMFC degradation under realistic driving cycle conditions : a local analysis and a basis for developing accelerated stress tests, Politecnico di Milano, 2021. http://hdl.handle.net/10589/175662.

[7] A. Bisello, E. Colombo, A. Baricci, C. Rabissi, L. Guetaz, P. Gazdzicki, A. Casalegno, Mitigated Start-Up of PEMFC in Real Automotive Conditions: Local Experimental Investigation and Development of a New Accelerated Stress Test Protocol, J. Electrochem. Soc. 168 (2021) 54501. https://doi.org/10.1149/1945-7111/abf77b.

[8] D.R. Baker, D.A. Caulk, K.C. Neyerlin, M.W. Murphy, Measurement of Oxygen Transport Resistance in PEM Fuel Cells by Limiting Current Methods, J. Electrochem. Soc. 156 (2009) B991. https://doi.org/10.1149/1.3152226.

[9] T.A. Greszler, D. Caulk, P. Sinha, The Impact of Platinum Loading on Oxygen Transport Resistance, J. Electrochem. Soc. 159 (2012) F831–F840. https://doi.org/10.1149/2.061212jes.

[10] C. Elena, C. Marco, C. Andrea, B. Andrea, B. Andrea, In-operando investigation of the degradation mechanisms during start-up/shut-down in PEMFC for automotive application, (2019).

[11] R. Makharia, M.F. Mathias, D.R. Baker, Measurement of Catalyst Layer Electrolyte Resistance in PEFCs Using Electrochemical Impedance Spectroscopy, J. Electrochem. Soc. 152 (2005) A970. https://doi.org/10.1149/1.1888367.

Key-words: Polymer electrolyte membrane fuel cell, Accelerated Stress Tests, automotive durability, catalyst layer degradation.

7. Acknowledgements

This work was developed in the framework of the European ID-FAST project, which has received funding from the Fuel Cells and Hydrogen 2 Joint Undertaking under European Union's Horizon 2020 research and innovation program (grant agreement No.779565).